Journal of Molecular Spectroscopy 370 (2020) 111298

Contents lists available at ScienceDirect

Journal of Molecular Spectroscopy

journal homepage: www.elsevier.com/locate/jms

Transition properties between low-lying electronic states of SiO^+

Zhi Qin [a,b,c], Tianrui Bai [a,b], Junming Zhao [c], Linhua Liu [a,b,c,*]

[a] Optics and Thermal Radiation Research Center, Shandong University, Qingdao 266237, China
[b] School of Energy and Power Engineering, Shandong University, Jinan 250062, China
[c] School of Energy Science and Engineering, Harbin Institute of Technology, Harbin 150001, China

ARTICLE INFO

Article history:
Received 24 February 2020
In revised form 28 April 2020
Accepted 29 April 2020
Available online 14 May 2020

Keywords:
Einstein coefficients
Oscillator strengths
Radiative lifetime
Spin-orbit couplings
SiO^+

ABSTRACT

In this work, we investigate the potential energy curves (PECs), transition dipole moments (TDMs) and spin-orbit couplings for low-lying electronic states of SiO^+ based on *ab initio* calculations. The PECs of seventeen low-lying electronic states are calculated by the internally contracted multireference configuration interaction (icMRCI) method with the Davidson correction, as well as the basis set extrapolation, core-valence (CV) correction and scalar relativistic correction. The Schrödinger equation of nuclear movement is solved over the PEC to obtain the rotational and vibrational energy levels, which are used to fit the spectroscopic parameters. The Einstein coefficients, Franck-Condon factors and oscillator strengths for dipole-allowed transitions are calculated with the PECs and TDMs. The radiative lifetimes of some excited states are also obtained. Our calculated radiative lifetime of 67.8 ns for $B^2\Sigma^+(v' = 0)$ is in excellent agreement with the recent experimental measurement of 66 ± 2 ns. The spin-orbit coupling integrals related to the $X^2\Sigma^+$, $A^2\Pi$, $B^2\Sigma^+$, $1^4\Sigma^+$, $1^4\Pi$ and $1^4\Sigma^-$ states are calculated using the Breit-Pauli Hamiltonian. In addition, the effects of spin-orbit couplings on the potential energies of the Λ-S electronic states are discussed.

1. Introduction

Silicon monoxide (SiO) is often formed from the ablated Si and O atoms in meteor entry [1] and has been observed in various stellar sources [2–10]. It is also an important participant on telluric chemistry [11]. Although its cation, SiO^+, has not been detected in the interstellar medium so far, it is easily generated from dissociative shocks under suitable conditions in dense clouds [12]. Therefore, the detailed knowledge of spectroscopy for SiO^+ is of great astrophysical interest. Two doublet electronic transition systems ($B^2\Sigma^+$-$X^2\Sigma^+$ and $B^2\Sigma^+$-$A^2\Pi$) have long been studied in the laboratory [13–22]. Experimental studies of spectra for SiO^+ initially used discharge spectroscopy [13–16,18], then photoelectron spectroscopy [17], and more recently fast-ion-beam laser spectroscopy [19–22], which can be utilized to measure more transition bands of SiO^+. For example, almost 1400 lines of the (0,0), (1,0), (1,1), (2,1), (2,2), (3,2) bands for the $B^2\Sigma^+$-$X^2\Sigma^+$ system and 66 lines of the (2,0) Ω = 1/2 sub-band for the $B^2\Sigma^+$-$A^2\Pi$ system [19,20], as well as the (4,4), (4,3), and (5,4) bands for the $B^2\Sigma^+$-$X^2\Sigma^+$ system and (3,2), (4,2), and (5,3) bands of the $B^2\Sigma^+$-$A^2\Pi$ system [22] have been observed by laser spectroscopy. In total, 2378 rovibronic transitions has been observed for the $B^2\Sigma^+$-$X^2\Sigma^+$ and $B^2\Sigma^+$-$A^2\Pi$ electronic transition systems in the laboratory.

Theoretically, a recent *ab initio* study of SiO^+ is provided by Li et al. [23], who investigated the electronic structures and transition properties of SiO^+ by the MRCI/aug-cc-pwCV5Z-DK method. Another recent *ab initio* study of SiO^+ is by Shi et al. [24], who presented a high-level study for the $X^2\Sigma^+$, $A^2\Pi$, $B^2\Sigma^+$, $a^4\Sigma^+$, $1^4\Pi$, $1^4\Delta$, $1^4\Sigma^-$, and $2^4\Pi$ electronic states of SiO^+ at the MRCI + Q/AV6Z + CV + DK level of theory. They just reported *ab initio* potential energies and spectroscopic parameters, along with the effect of spin-orbit coupling on the spectroscopic parameters. In addition, a relatively recent *ab initio* study of SiO^+ is by Chattopadhyaya et al. [25], who used the multireference singles and doubles configuration interaction (MRDCI) method to calculate potential energy, spectroscopic parameters and transition dipole moments (TDMs) for low-lying electronic states of SiO^+. Earlier, but comprehensive, *ab initio* studies of SiO^+ were performed by Cai and Francois [26,27] using the internally contracted multireference configuration interaction (MRCI) method for investigating low-lying electronic states of SiO^+. However, oscillator strengths and spin-orbit coupling integrals between different electronic states have not been widely reported before, but are very important to accurately describe the spectra of SiO^+.

* Corresponding author at: Optics and Thermal Radiation Research Center, Shandong University, Qingdao 266237, China.
E-mail address: liulinhua@sdu.edu.cn (L. Liu).

https://doi.org/10.1016/j.jms.2020.111298
0022-2852/

Recently, experimental investigations of the $B^2\Sigma^+$-$X^2\Sigma^+$ (0,0) transition of SiO^+ were carried out by Stollenwerk et al. [28] due to its implications for laser cooling. In the past few years, laser-cooling and magneto-optical trapping have been extended to diatomic molecules and molecular ions [29–32]. Cold and ultracold molecules and ions are of growing interest because of their potential applications of quantum information and simulation [33–35], cold controlled chemistry [36,37], precise measurements [38,39], etc., which motivates researchers to search for candidates for laser cooling. Experiments of laser cooling have been successfully carried out for the SrF [29,40], KRb [41], YO [30], and CaF [42], and theoretically possible laser cooling schemes have been proposed for RaF [38], AlH [43], AlF [43], BeF [44], LiRb [45], and TlCl [46] etc. Except for the neutral diatomic molecules, molecular ions, such as C_2^- [32], BH^+ [47], AlH^+ [47], $AlCl^+$ [48], GaH^+ [49], and InH^+ [49], were found to be prospective candidates for laser cooling. In 2011, Nguyen and Odom proposed a three-electronic-level laser cooling scheme for SiO^+, along with the discussion of other candidate three-electronic-level molecules. Recently, a viable optical cycling scheme based on the $B^2\Sigma^+$-$X^2\Sigma^+$ transition of SiO^+ has been presented by Li et al. [23].

In this paper, we present a systematic investigation of the electronic structure and transition properties of SiO^+ by the state-of-the-art *ab initio* method as implemented in the MOLPRO 2015 package [50]. The aim of this work is threefold. Firstly, this work is to present a more detailed study on the electronic structures of SiO^+, including the potential energy curves (PECs) and spectroscopic parameters of low-lying electronic states. The second purpose is to provide the transition properties of SiO^+, including the transition dipole moments (TDMs), Franck-Condon factors (FCFs), Einstein *A* coefficients, oscillator strengths and spontaneous radiative lifetimes of dipole allowed transitions. The third intension is to investigate the spin-orbit couplings within the spin-orbit selection rule and their effects on the potential energies of Λ-S states.

This paper is organized as follows. The state-of-the-art *ab initio* method is detailed in Section 2. The computational results, including the electronic structures, transition properties and spin-orbit coupling integrals for SiO^+, are presented and discussed in Section 3. Finally, in Section 4, a brief summary is given.

2. Computational method

The electronic structure calculations of SiO^+ were performed using the state-averaged complete active space self-consistent field (SA-CASSCF) [51,52], followed by the internally contracted multireference configuration interaction (icMRCI) method [53,54] with the Davidson correction (+Q). We described the Si and O atoms with the aug-cc-pV6Z basis set [55–57] for the main electronic structure calculations. In order to obtain more accurate potential energy, the basis-set extrapolation to the complete basis set (CBS) limit was considered with the aug-cc-pV5Z and aug-cc-pV6Z basis sets [55–57]. We used the basis-set extrapolation formulas given by Truhler [58]

$$E_X^{ref} = E_\infty^{ref} + A^{ref}X^{-\alpha}, \tag{1}$$

$$E_X^{cor} = E_\infty^{cor} + A^{cor}X^{-\beta}. \tag{2}$$

where E_X^{ref} and $E^{cor}{}_X$ are the reference and correlation energies of an electronic state at a certain internuclear distance, respectively, calculated with the aug-cc-pVXZ (here X = 5 and 6) basis set. E_∞^{ref} and E_∞^{cor} denote the reference and correlation energies, respectively, which are both obtained by the extrapolation of the basis set to the CBS limit. The extrapolation parameters α and β are equal to 3.4 and 2.4 for the reference energy and correlation energy, respectively. The extrapolation results are denoted as "56" for convenience.

Core-valence correction was considered with the cc-pCV5Z basis set [56] at the icMRCI level of theory. The method used here was described in detail in a previous publication of Peterson and Dunning [59]. According to this method, two electrons in the 1s inner orbital of a Si^+ cation were frozen when we performed the core-valence correlation calculation. When we performed the frozen-core calculation, ten electrons in the 1*s*2*s*2*p* inner orbitals of a Si^+ cation and two electrons in the 1*s* inner orbital of an O atom were frozen. The difference of the energies obtained by these two calculations is the contribution to the total energy by the core-valence correction. Such contribution is denoted as "CV" for convenience.

Scalar relativistic correction was also taken into account with the cc-pV5Z-DK basis set [60] at the icMRCI level of theory. Based on the approach presented by Jong et al. [60], the potential energy of a certain electronic state was calculated, respectively, using third-order Douglas-Kroll-Hess Hamiltonian approximation [61,62] with the cc-pV5Z-DK basis set [60] and using only the cc-pV5Z basis set. The difference between these two energies is the contribution to the total energy by the scalar relativistic correction and is represented as "DK". So the final potential energies are obtained at the icMRCI + Q/56 + CV + DK level of theory. Similar treatments have been used in our previous publications [63–65] and by many other theoretical groups [66–68]. The SOC integrals between low-lying electronic states of SiO^+ are evaluated using the Breit-Pauli Hamiltonian [69] at the CASSCF/MRCI/AV6Z level of theory.

Calculations were carried out in C_{2v} point group. Nine electrons were put into 9 outermost orbitals, which constituted the active space: five a_1 orbitals, two b_1 orbitals, two b_2 orbitals (noted as 5,2,2,0), corresponding to the Si 3*s*3*p* and O 2*p* shells. The remaining electrons in the Si 1s2s2p and O 1s shells were put into the closed space: four a_1 orbitals, one b_1 orbital, one b_2 orbital.

The nuclear motion problem was then solved based on the PECs to determine the spectroscopic parameters. The PECs and TDM curves were used with the LEVEL program of Le Roy [70] to obtain the transition probabilities, including FCFs $q_{\upsilon'\upsilon''}$, Einstein *A* coefficients $A_{\upsilon'\upsilon''}$ and absorption band oscillator strengths $f_{\upsilon'\upsilon''}^{abs}$, which can be calculated by

$$q_{\upsilon'\upsilon''} = \left(\int \psi_{\upsilon'}(r)\psi_{\upsilon''}(r)dr\right)^2 \tag{3}$$

$$A_{\upsilon'\upsilon''} = 2.026\times10^{-6}\sigma_{\upsilon'\upsilon''}^3\frac{2-\delta_{0,\Lambda'+\Lambda''}}{2-\delta_{0,\Lambda'}}\left(R_e^{\upsilon'\upsilon''}\right)^2 \tag{4}$$

$$f_{\upsilon'\upsilon''}^{abs} = 3.0376\times10^{-6}\sigma_{\upsilon'\upsilon''}\frac{2-\delta_{0,\Lambda'+\Lambda''}}{2-\delta_{0,\Lambda'}}\left(R_e^{\upsilon'\upsilon''}\right) \tag{5}$$

where $\psi_{\upsilon'}$ and $\psi_{\upsilon''}$ are the vibrational wave functions, respectively, corresponding to the vibrational level of the upper electronic state υ' and the vibrational level of the lower state υ'', *r* is the internuclear distance, $\sigma_{\upsilon'\upsilon''}$ is the wavenumber, Λ' and Λ'' are the projections of electronic orbital angular momentums on the internuclear axis for the upper and lower electronic levels, respectively. $\left(R_e^{\upsilon'\upsilon''}\right)^2$ is the square of the electronic-vibrational transition moment, given by

$$\left(R_e^{\upsilon'\upsilon''}\right)^2 = \left[\int_0^\infty \psi_{\upsilon'}(r)R_e(r)\psi_{\upsilon''}(r)dr\right]^2 \tag{6}$$

where $R_e(r)$ is the TDM function. The radiative lifetimes $\tau_{\upsilon'}$ can be computed by

$$\tau_{\upsilon'} = \frac{1}{\sum_{\upsilon''=0}^{\upsilon''_{max}} A_{\upsilon'\upsilon''}} \tag{7}$$

where v''_{max} is the maximum vibrational quantum number considered in the lower electronic state.

3. Results and discussions

3.1. Electronic structure

In this work, the icMRCI + Q/56 + CV + DK method is used to calculate the potential energies of the electronic states of SiO^+ from 1 to 12 Å. we consider seventeen low-lying electronic states of SiO^+, which are shown in Fig. 1. For better clarity, we present the PECs of doublet and quartet electronic states in Fig. 2(a) and (b), respectively, from 1 to 4 Å. The PECs of these electronic states from 1 to 12 Å are given in the supplemental material. The dissociation relationships of these seventeen electronic states are presented in Table 1. The twelve electronic states that converge to the O [$(2s^22p^4)$ ^3P_g] + Si^+[$(3s^23p)$ ^2P_u] dissociation limit are all considered. The $B^2\Sigma^+$ and $2^2\Delta$ electronic states correspond to the O [$(2s^22p^4)$ ^1D_g] + Si^+[$(3s^23p)$ ^2P_u] dissociation limit. Moreover, we identify three new bound electronic states ($2^4\Sigma^+$, $3^4\Pi$, and $2^2\Delta$), which correlate to the O[$(2s^22p^4)$ ^3P_g] + Si^+[$(3s3p^2)$ ^4P_u] dissociation limit and have not been available in previous publications. The energy separations between different dissociation limits are obtained by the energy differences between the energies of the electronic states dissociated the corresponding limits at a large internuclear distance of 12 Å. As shown in Table 1, our computed energy separations between different dissociation limits agree well with the experimental values [71]. As for the experimental values, we have made a weighted average between energies of the $O(^3P_2)$, $O(^3P_1)$ and $O(^3P_0)$ states and then obtained an equivalent value served as the energy of $O(^3P_u)$ state. Similarly, we have made a weighted average of the energies of the $Si^+(^2P_{1/2})$ and $Si^+(^2P_{3/2})$ states and then obtained an equivalent value acted as the energy of the $Si^+(^2P_u)$ state. We have also made a weighted average of the energies of the $Si^+(^4P_{1/2})$, $Si^+(^4P_{3/2})$ and $Si^+(^4P_{5/2})$ states and then obtained an equivalent value regarded as the energy of the $Si^+(^4P_u)$ state.

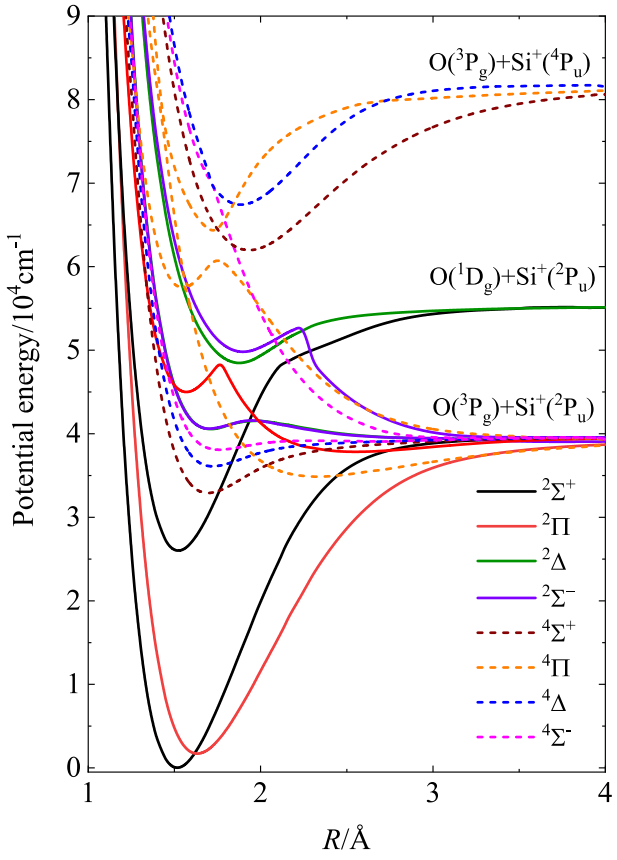

Fig. 1. Potential energy curves of the electronic states of SiO^+ at the icMRCI + Q/56 + CV + DK level of theory. These states are given in energy relative to the minimum energy of the ground state of SiO^+.

Based on the PECs, we determine the spectroscopic parameters of the bound electronic states considered here, including adiabatic excitation energy T_e, equilibrium internuclear distance R_e, vibrational constant ω_e and $\omega_e\chi_e$, rotational constant B_e, and rovibrational coupling constant α_e. The results are listed in Table 2, together with previous experimental and theoretical ones. Experiments only identified the $X^2\Sigma^+$, $A^2\Pi$, and $B^2\Sigma^+$ electronic states of SiO^+. Before comparing with the experimental results of the spectroscopic parameters, we should note that our results are similar to those reported by Cai and Francois [27], Chattopadhyaya et al. [25], Shi et al. [24] and Li et al. [23]. However, different levels of theory and basis sets still have a slight effect on the PECs near equilibrium for the states studied here, which indeed affects the transition properties and radiative lifetimes reported below. Detailed comparisons and analysis show that our calculated spectroscopic parameters are closer to those computed by Shi et al. [24]. Compared with the experimental spectroscopic parameters for the $X^2\Sigma^+$, $A^2\Pi$, and $B^2\Sigma^+$ electronic states, our results and the calculations of Shi et al. [24] are closer to the experimental ones than other theoretical results [23,25–27]. By comparing these theoretical papers, we found that both our work and the work of Shi et al. [24] considered the CV correction, while others did not consider such correction. So we suspect that CV correction is very important in describing the potential energy of electronic states.

At the icMRCI + Q/56 + CV + DK level of theory, the equilibrium internuclear distance R_e of the ground state is calculated to be 1.5158 Å, which differs by 0.0004 Å from the experimental value given by Rosner et al. [22]. Our calculated ω_e is larger than the experimental value of Rosner et al. by about 6 cm^{-1}. The D_e value is computed to be 39552.59 cm^{-1}, which is closer to the experimental value of 40166.39 cm^{-1} measured by Colbourn et al. [17] than previous theoretical value of 38230.66 cm^{-1} [27]. For other spectroscopic parameters, a good agreement with the experiment ones is also observed. For the $A^2\Pi$ electronic state, our calculated ω_e of 949.9 cm^{-1} is larger than the theoretical values of 933.2 cm^{-1}, 923 cm^{-1} and 929 cm^{-1} computed by Cai and Francois [27], Chattopadhyaya et al. [25] and Li et al. [23], respectively, but closer to the recent experimental value of 946.28 cm^{-1} [22]. Similar results are also found by comparing other spectroscopic parameters except for T_e. Our icMRCI + Q/56 + CV + DK method does not reproduce the T_e value well. Instead, the T_e value calculated by Shi et al. [24], which likewise considered the CV correlation, is in better agreement with the experimental value measured by Rosner et al. [22]. We employ the experimental T_e value of the $A^2\Pi$ state in the subsequent investigation of the $A^2\Pi$-$X^2\Sigma^+$ and $B^2\Sigma^+$-$A^2\Pi$ transition properties. For the $B^2\Sigma^+$ electronic state, the calculated T_e, ω_e, and R_e are 25987.01 cm^{-1}, 1148.90 cm^{-1}, and 1.5221 Å, respectively, which well reproduce the experiment with a deviation of 42 cm^{-1} for T_e, 12 cm^{-1} for ω_e, and 0.0049 Å for R_e.

The PECs of the $2^4\Sigma^+$, $3^4\Pi$, and $2^2\Delta$ electronic states are reported for the first time. By using the MRCI/aug-cc-PV6Z method, we calculate the electronic configurations of these three electronic states. The wavefunctions of the $2^4\Sigma^+$ electronic state are dominated by (core)$5\sigma^26\sigma^12\pi^37\sigma^23\pi^1$(52%) and (core)$5\sigma^26\sigma^22\pi^27\sigma^13\pi^2$(29%) near its equilibrium internuclear distance. The $3^4\Pi$ electronic state is described by the electronic configurations of (core)$5\sigma^26\sigma^22\pi^37\sigma^18\sigma^1$ (53%) and (core)$5\sigma^26\sigma^12\pi^47\sigma^13\pi^1$(36%) near its equilibrium internuclear distance. For the $2^2\Delta$ electronic state, its wavefunction is represented

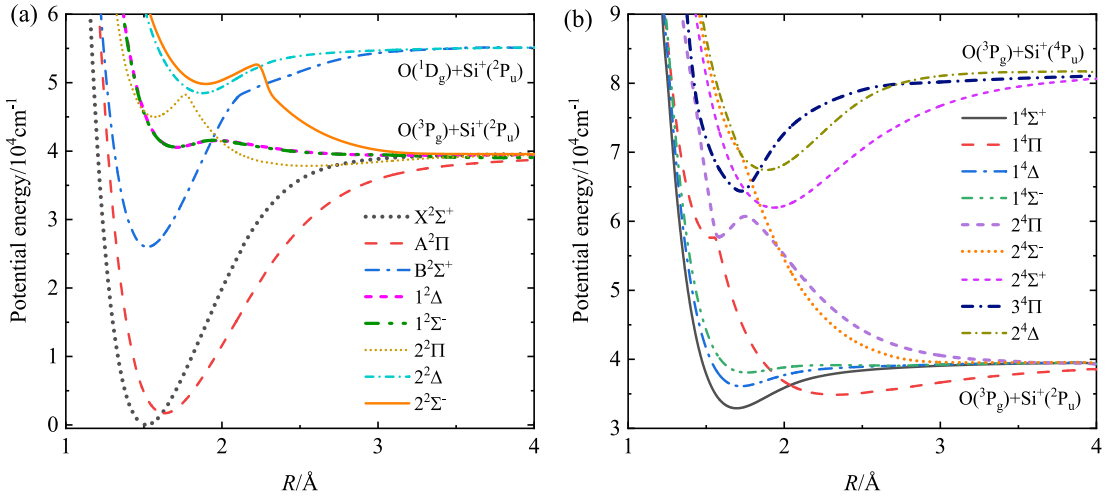

Fig. 2. Potential energy curves of (a) the doublet electronic states and (b) the quartet states of SiO^+.

Table 1
Dissociation relationships of 17 low-lying electronic states of SiO^+ resulting from three dissociation limits.

Dissociation limit	Electronic state	Relative energy (cm^{-1})	
		This work[a]	Exp. [71].
O[($2s^22p^4$) ^3P_g] + Si$^+$[($3s^23p$) ^2P_u]	$1^4\Sigma^+$, $1^4\Sigma^-$, $2^4\Sigma^-$, $1^4\Pi$, $2^4\Pi$, $1^4\Delta$, $X^2\Sigma^+$, $1^2\Sigma^-$, $2^2\Sigma^-$ $A^2\Pi$, $2^2\Pi$, $1^2\Delta$	0	124.565[b]
O[($2s^22p^4$) ^1D_g] + Si$^+$[($3s^23p$) ^2P_u]	$B^2\Sigma^+$, $2^2\Delta$	15,629	15939.672[c]
O[($2s^22p^4$) ^3P_g] + Si$^+$[($3s3p^2$) ^4P_u]	$2^4\Sigma^+$, $3^4\Pi$, $2^4\Delta$	42,238	43007.695[d]

[a] Obtained by the icMRCI + Q/56 + CV + DK calculations.
[b] Obtained by summing over the weighted average energy of the O($^3P_2$), O($^3P_1$) and O($^3P_0$) states and that of the Si$^+$($^2P_{1/2}$) and Si$^+$($^2P_{3/2}$) states.
[c] Obtained by summing over the energy of the O($^1D_2$) state and the weighted average energy of the Si$^+$($^2P_{1/2}$) and Si$^+$($^2P_{3/2}$) states.
[d] Obtained by summing over the weighted average energy of the O($^3P_2$), O($^3P_1$) and O($^3P_0$) states and that of the Si$^+$($^4P_{1/2}$), Si$^+$($^4P_{3/2}$) and Si$^+$($^4P_{5/2}$) states.

by (core)$5\sigma^26\sigma^12\pi^37\sigma^23\pi^1$ (60%), (core)$5\sigma^26\sigma^12\pi^33\pi^18\sigma^1$ (17%) and (core)$5\sigma^26\sigma^22\pi^27\sigma^13\pi^2$(15%).

3.2. Transition properties and radiative lifetimes

The TDMs for dipole allowed transitions of SiO^+ are shown in Figs. 3–5. An example of the Einstein *A* coefficients, Franck-Condon factors and absorption band oscillator strengths is listed in Tables 3–5 for the $A^2\Pi$-$X^2\Sigma^+$, $B^2\Sigma^+$-$X^2\Sigma^+$ and $B^2\Sigma^+$-$A^2\Pi$ electronic transition systems, respectively. These transition quantities for other electronic systems are given in the supplemental material. Table 6 presents the radiative lifetimes of four lowest vibrational levels for the $B^2\Sigma^+$ electronic state of SiO^+. Its radiative lifetimes are dominantly determined by decay to the $X^2\Sigma^+$ electronic state, which is not too surprising as the TDM of the $B^2\Sigma^+$-$X^2\Sigma^+$ system is much larger than that of the $B^2\Sigma^+$-$A^2\Pi$ electronic transition system in the Franck-Condon region. A slight slow decrease in the radiative lifetime with the increasing v' is observed. Although this is inconsistent with the experiment [21] and other theoretical calculations [23,25,27], which exhibit a slight slow increase in radiative lifetime with increasing v', the difference between our radiative lifetimes and those given by experiments and calculations is still small and theoretically reasonable. More importantly, the radiative lifetime of 67.8 ns for $v' = 0$ is in better agreement with the recent experimental measurement of 66 ± 2 ns [28] than other theoretical results [23,25,27]. Such a better agreement is probably due mainly to higher level of theory in calculating the PECs in this work.

The $A^2\Pi$ electronic state was identified experimentally by the $B^2\Sigma^+$-$A^2\Pi$ transition. The $A^2\Pi$-$X^2\Sigma^+$ transition spectrum has not been measured in the laboratory, which is mainly because of relatively weak spectral intensity for the $A^2\Pi$-$X^2\Sigma^+$ transition. The Einstein *A* coefficients are calculated to be 8.38×10^3, 9.97×10^3, 4.77×10^3, 9.34×10^3, 1.13×10^4 s^{-1} for the (3,0), (4,0), (4,1), (5,0), and (5,1) bands, respectively. These bands are strong enough that can be hopefully observed by an appropriate spectroscopy. However, the bands corresponding to $A^2\Pi$ ($v' \leq 2$)-$X^2\Sigma^+$ have relatively weak transition probabilities, resulting in large radiative lifetimes for $v' \leq 2$ of the $A^2\Pi$ electronic state (as shown in Table 6).

In addition to the $B^2\Sigma^+$ and $A^2\Pi$ electronic states, we also evaluate the radiative lifetimes of the $1^2\Delta$, $1^2\Sigma^-$, $2^2\Sigma^-$, $2^2\Delta$, $2^4\Sigma^+$, $2^4\Delta$, and $2^2\Pi$ electronic states, shown in Tables 7 and 8. The small TDMs in the Franck-Condon region and the large R_e difference between the $1^4\Pi$ electronic state and the $1^4\Sigma^+$, $1^4\Delta$, and $1^4\Sigma^-$ electronic states lead to very small transition probabilities. Hence, the transition properties for the $1^4\Pi$-$1^4\Sigma^+$, $1^4\Delta$-$1^4\Pi$, and $1^4\Sigma^-$-$1^4\Pi$ electronic transition systems are not discussed here. The radiative lifetimes for the $1^2\Delta$ and $1^2\Sigma^-$ electronic states are very similar, which are determined by decay to the $A^2\Pi$ electronic state. For the $1^2\Delta$ and $1^2\Sigma^-$ electronic states, 65% of the wave function is described by the configuration (core)$5\sigma^26\sigma^22\pi^37\sigma^13\pi^1$, and 20% of the wave function is described by the configuration (core) $5\sigma^2$-$6\sigma^12\pi^37\sigma^23\pi^1$. That is, the $1^2\Delta$-$A^2\Pi$ and $1^2\Sigma^-$-$A^2\Pi$ electronic transition systems correspond to $3\pi \rightarrow 7\sigma$ transition and $3\pi \rightarrow 6\sigma$ transition, respectively. Of course, the energy separations of these two transitions are different, leading to the difference in the radiative lifetimes of the $1^2\Delta$ and $1^2\Sigma^-$ states, but they are of the same order of magnitude. A similar phenomenon can also be found by comparing the $2^2\Sigma^-$-$A^2\Pi$ system with the $2^2\Delta$-$A^2\Pi$ system.

Table 2
Spectroscopic parameters of the bound electronic states for SiO^+ considered in this work.

State		D_e/cm^{-1}	T_e/cm^{-1}	R_e/Å	ω_e/cm^{-1}	$\omega_e\chi_e$/cm^{-1}	B_e/cm^{-1}	$10^3\alpha_e$/cm^{-1}
$X^2\Sigma^+$	This work	39,553	0.00	1.5158	1168	9.84	0.7206	4.84
	Exp. [17]	40166.39	0.00	1.512	1120			
	Exp. [18]		0.00		1164		0.71762	
	Exp. [20]		0.00		1161.97	6.8718	0.72055	5.8872
	Exp. [22]		0.00	1.5162	1162.18	6.9698	0.72062	5.87114
	Cal. [27]	38,231	0.00	1.5295	1167	8.15	0.70785	
	Cal. [25]		0.00	1.538	1125			
	Cal. [24]		0.00	1.5173	1158	6.99	0.71948	5.86
	Cal. [23]	39,198	0.00	1.5228	1148	6.5	0.7143	
$A^2\Pi$	This work	37,906	1625	1.6319	951	6.33	0.6220	4.99
	Exp. [17]	39279.18		1.645	1030			
	Exp. [20]		2133.01		944.1	5.0	0.6189	4.0
	Exp. [22]		2242.25	1.636	946.28	7.005	0.61859	4.71
	Cal. [27]	36,376	1879	1.6643	933	5.93	0.61282	2.86
	Cal. [25]		790	1.656	923			
	Cal. [24]		2183	1.6342	947	6.54	0.62009	4.86
	Cal. [23]		2201	1.6430	929	5.0	0.6137	
$B^2\Sigma^+$	This work	29,195	25,987	1.5221	1149	6.76	0.7150	5.63
	Exp. [17]			1.545	1180			
	Exp. [18]		26016.58		1138		0.71076	
	Exp. [20]		26016.27		1136.60	6.9202	0.71302	
	Exp. [22]		26029.01	1.527	1136.58	6.9215	0.71304	5.81
	Cal. [27]	28,552	25,722	1.5391	1125	7.22	0.69945	2.99
	Cal. [25]	25,484		1.546	1107			
	Cal. [24]		25,998	1.5195	1137	14.6	0.71757	4.68
	Cal. [23]		25,577	1.5329	1122	6.7	0.7048	
$1^4\Sigma^+$	This work	6658	32,899	1.6941	721	15.7	0.5750	7.61
	Cal. [27]	6210	31,984	1.7100	712	15.4	0.56581	2.89
	Cal. [25]		30,493	1.727	673			
	Cal. [24]		34,038	1.6990	714	13.5	0.57446	11.8
	Cal. [23]		32,228	1.7032	760	22.2	0.5717	
$1^4\Pi$	This work	4625	34,861	2.3265	274	7.25	0.3071	6.70
	Cal. [27]	4275	33,959	2.3841	302	5.71	0.29078	2.02
	Cal. [25]		30,650	2.454	284			
	Cal. [24]		35,292	2.3204	271	3.51	0.30762	4.91
	Cal. [23]		34,618	2.3373	264	3.9	0.3032	
$1^4\Delta$	This work	3482	36,098	1.7216	640	36.7	0.5701	22.31
	Cal. [27]	2823	35,391	1.7451	573	12.8	0.54337	2.92
	Cal. [25]		33,957	1.768	547			
	Cal. [24]		35,784	1.7207	630	17.4	0.55927	1.23
	Cal. [23]		35,319	1.7294	620	26.3	0.5550	
$1^4\Sigma^-$	This work	1479	38,085	1.7590	493	35.7	0.5387	32.1
	Cal. [27]	968	37,277	1.7893	460	22.1	0.51788	2.86
	Cal. [25]		35,574	1.823	439			
	Cal. [24]		37,656	1.7508	544	24.0	0.53934	1.43
	Cal. [23]		37,185	1.7580	431	23.0	0.5367	
$1^2\Delta$	This work	988	40,553	1.7030	703	47.4	0.5709	36.3
	Cal. [27]		40,785	1.7319	561		0.53933	3.04
	Cal. [25]		39,530	1.764	538			
	Cal. [23]		40,030	1.7107	666	54.2	0.5809	
$1^2\Sigma^-$	This work	1008	40,597	1.7090	710	70.6	0.5746	39.8
	Cal. [27]		40,760	1.7280	508		0.53112	3.16
	Cal. [25]		39,611	1.776	522			
	Cal. [23]		40,177	1.7184	645	52.5	0.5719	
$2^2\Pi$	This work	3405	44,966	1.5686	993	3.46	0.6718	3.33
	Cal. [27]		44,680	1.5768	913	15.1	0.66698	3.86
	Cal. [25]		44,371	1.604	917			
	Cal. [24]		44,469	1.5750	985	8.12	0.66773	0.66
	Cal. [23]		43,907	1.5817	979	14.5	0.6624	
State		D_e/cm^{-1}	T_e/cm^{-1}	R_e/Å	ω_e/cm^{-1}	$\omega_e\chi_e$/cm^{-1}	B_e/cm^{-1}	$10^3\alpha_e$/cm^{-1}
$2^2\Delta$	This work	6730	48,467	1.8764	681	13.5	0.4682	0.60
	Cal. [27]	6049	48,229	1.8810	578	7.13	0.46820	2.36
	Cal. [25]		47,198	1.881	615			
	Cal. [23]		47,819	1.8759	651	15.9	0.4702	
$2^2\Sigma^-$	This work	3450	49,803	1.8967	635	15.7	0.4614	3.90
	Cal. [27]		49,275	1.8989	644	11.1	0.45935	2.34
	Cal. [25]		48,234	1.924	728			
	Cal. [23]		47,859	1.8764	692	17.6	0.4703	

(*continued on next page*)

Table 2 (*continued*)

State		D_e/cm^{-1}	T_e/cm^{-1}	R_e/Å	ω_e/cm^{-1}	$\omega_e\chi_e$/cm^{-1}	B_e/cm^{-1}	$10^3\alpha_e$/cm^{-1}
$2^4\Sigma^+$	This work	19,743	61,977	1.9332	631	4.14	0.4433	2.64
$3^4\Pi$	This work	17,396	64,322	1.7247	1293	46.7	0.5597	5.94
$2^4\Delta$	This work	14,369	67,421	1.8848	673	0.52	0.4685	4.19

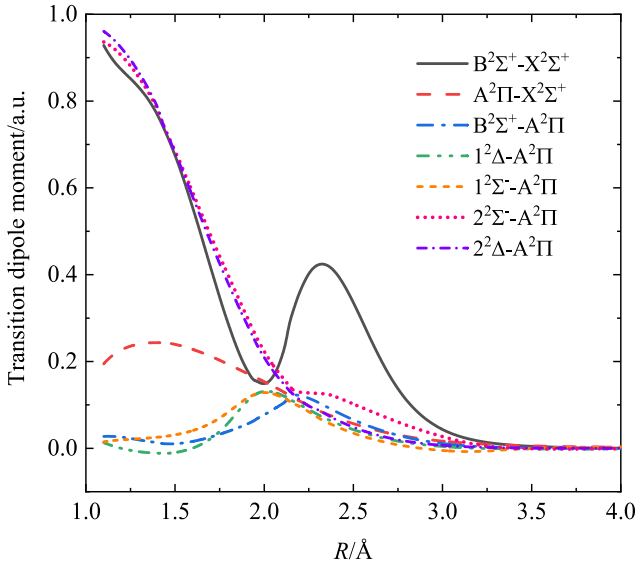

Fig. 3. The TDM curves for the transitions used to compute the radiative lifetimes of the $B^2\Sigma^+$, $A^2\Pi$, $1^2\Delta$, $1^2\Sigma^-$, $2^2\Sigma^-$, and $2^2\Delta$ electronic states. The $1^2\Delta$-$A^2\Pi$ and $2^2\Delta$-$A^2\Pi$ moments are the Cartesian moment $\langle\Pi_x|y|\Delta_{xy}\rangle$, where $\left\langle\Pi\left|\frac{x+iy}{\sqrt{2}}\right|\Delta\right\rangle = \sqrt{2}\langle\Pi_x|y|\Delta_{xy}\rangle$.

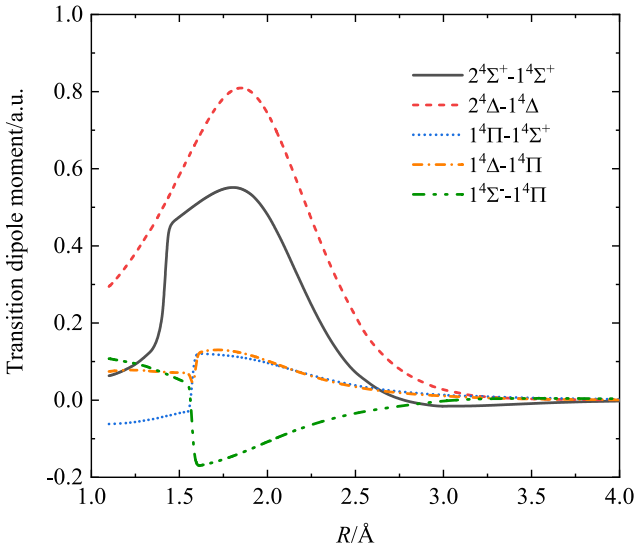

Fig. 5. The TDM curves for transitions used to compute the radiative lifetimes of the $1^4\Pi$, $1^4\Delta$, $1^4\Sigma^-$, $2^4\Sigma^+$, and $2^4\Delta$ electronic states. The $1^4\Delta$-$1^4\Pi$ moment are the Cartesian moment $\langle\Pi_x|y|\Delta_{xy}\rangle$, where $\left\langle\Pi\left|\frac{x+iy}{\sqrt{2}}\right|\Delta\right\rangle = \sqrt{2}\langle\Pi_x|y|\Delta_{xy}\rangle$.

Recent interest in SiO^+ is motivated by its properties that can be exploited for direct laser cooling and magneto-optical trapping. In 2011, Nguyen and Odom [72] discussed Doppler cooling of three-electronic-level molecules and determined that Doppler cooling of SiO^+ can be achieved without optically repumping from the intermediate state. Then, they performed experimental investigations of spectroscopy of SiO and SiO^+ to observe the electronic states above the $B^2\Sigma^+$ state, thus achieving Doppler cooling of SiO^+. Some research findings were achieved in the subsequent few years. For example, Stollenwerk et al. [28] measured the electronic spectroscopy of SiO^+ for laser cooling of a trapped sample of SiO^+. In their work, the radiative branching ratio of SiO^+ was firstly measured using laser induced fluorescence (LIF). they also recorded the 1 + 1 resonance-enhanced multiphoton ionization (1 + 1 REMPI) spectrum of SiO in the 210–220 nm range for SiO^+ ion trap loading [73]. Good candidates for direct laser cooling in a closed-loop cycle need two particular criteria: highly diagonal FCFs and a short radiative lifetime. Based on the MRCI/aug-cc-pwCV5Z-DK calculations, Li et al. [23] provided a laser cooling scheme for SiO^+ molecule using the $B^2\Sigma^+$-$X^2\Sigma^+$ transition. We do not provide a new laser cooling scheme but provide the transition properties for supporting laser cooling studies. The spectroscopic parameters and transition properties calculated above can provide theoretical reference for observing the electronic states above the $B^2\Sigma^+$ state and seeking for possible laser cooling schemes. For ease of use, the branching ratio $b_{v'v''}$ is predicted by

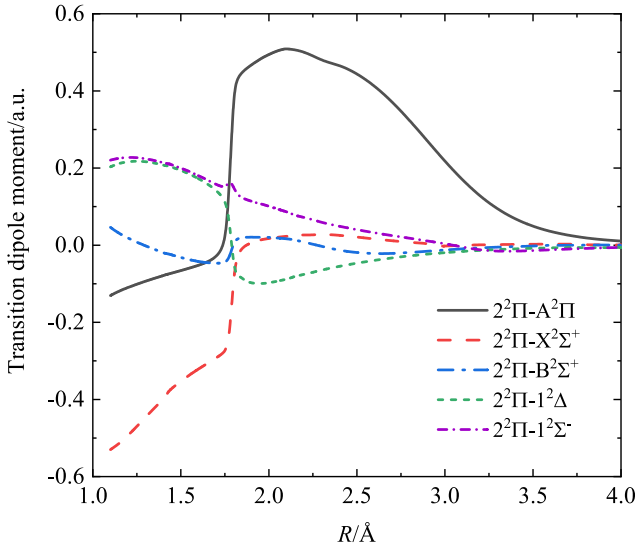

Fig. 4. The TDM curves for transitions used to compute the radiative lifetimes of the $2^2\Pi$ electronic state. The $2^2\Pi$-$1^2\Delta$ moment are the Cartesian moment $\langle\Pi_x|y|\Delta_{xy}\rangle$, where $\left\langle\Pi\left|\frac{x+iy}{\sqrt{2}}\right|\Delta\right\rangle = \sqrt{2}\langle\Pi_x|y|\Delta_{xy}\rangle$.

$$b_{v'v''} = \frac{A_{v'v''}}{\sum_{v''} A_{v'v''}} \tag{8}$$

Table 9 compares our Franck-Condon factors and branching ratios with those measured by Stollenwerk et al. [28] and Cameron et al. [19] and calculated by Li et al. [23].

3.3. Spin-orbit couplings

Fig. 6 displays the spin-orbit coupling terms between low-lying electronic states of interest for SiO^+, calculated by the CASSCF/

Table 3
Einstein *A* coefficients (first row), Franck-Condon factors (second row) and absorption band oscillator strengths (third row) for the $A^2\Pi$-$X^2\Sigma^+$ electronic transition system.

	v''				
v'	0	1	2	3	4
0	1.67×10^{2}	2.45×10^{1}			
	1.15×10^{-1}	2.77×10^{-1}	2.97×10^{-1}	1.89×10^{-1}	7.90×10^{-2}
	8.86×10^{-5}	8.20×10^{-5}	-4.10×10^{-5}	-9.92×10^{-5}	-6.77×10^{-5}
1	1.64×10^{3}	3.01×10^{2}	3.01×10^{-2}	-3.21×10^{-2}	-7.08×10^{1}
	2.17×10^{-1}	1.49×10^{-1}	0.00×10^{0}	1.17×10^{-1}	2.31×10^{-1}
	2.95×10^{-4}	1.28×10^{-4}	5.78×10^{-8}	-4.56×10^{-6}	-9.68×10^{-5}
2	4.96×10^{3}	7.36×10^{1}	2.90×10^{2}	3.73×10^{1}	0.00×10^{0}
	2.29×10^{-1}	8.01×10^{-3}	1.09×10^{-1}	9.72×10^{-2}	1.01×10^{-3}
	4.48×10^{-4}	1.18×10^{-5}	1.02×10^{-4}	4.69×10^{-5}	7.49×10^{-8}
3	8.38×10^{3}	6.40×10^{2}	1.15×10^{3}	8.49×10^{0}	7.70×10^{1}
	1.78×10^{-1}	2.71×10^{-2}	1.09×10^{-1}	3.01×10^{-3}	1.21×10^{-1}
	4.58×10^{-4}	5.38×10^{-5}	1.65×10^{-4}	2.50×10^{-6}	6.80×10^{-5}
4	9.97×10^{3}	4.77×10^{3}	5.62×10^{2}	9.91×10^{2}	1.54×10^{2}
	1.15×10^{-1}	9.51×10^{-2}	2.10×10^{-2}	8.28×10^{-2}	3.41×10^{-2}
	3.67×10^{-4}	2.48×10^{-4}	4.40×10^{-4}	1.28×10^{-4}	3.84×10^{-5}

Table 4
Einstein *A* coefficients (first row), Franck-Condon factors (second row) and absorption band oscillator strengths (third row) for the $B^2\Sigma^+$-$X^2\Sigma^+$ electronic transition system.

	v''				
v'	0	1	2	3	4
0	1.48×10^{7}	3.41×10^{4}	6.80×10^{2}	5.87×10^{0}	7.27×10^{-1}
	9.77×10^{-1}	7.01×10^{-3}	7.03×10^{-7}	8.76×10^{-8}	1.15×10^{-7}
	3.25×10^{-2}	8.39×10^{-6}	1.88×10^{-6}	1.83×10^{-8}	2.58×10^{-9}
1	4.09×10^{5}	1.44×10^{7}	7.10×10^{3}	2.50×10^{3}	4.25×10^{1}
	7.01×10^{-3}	9.62×10^{-1}	1.51×10^{-2}	4.68×10^{-7}	1.02×10^{-6}
	7.92×10^{-4}	3.09×10^{-2}	1.70×10^{-5}	6.72×10^{-6}	1.28×10^{-6}
2	6.17×10^{3}	8.47×10^{7}	1.40×10^{7}	1.23×10^{4}	5.8×10^{3}
	8.67×10^{-5}	1.40×10^{-2}	9.46×10^{-1}	2.40×10^{-2}	4.93×10^{-9}
	1.06×10^{-5}	1.61×10^{-3}	2.94×10^{-2}	2.89×10^{-5}	1.52×10^{-5}
3	1.08×10^{2}	2.19×10^{4}	1.32×10^{6}	1.35×10^{7}	1.74×10^{4}
	2.56×10^{-6}	3.14×10^{-4}	2.30×10^{-2}	9.28×10^{-1}	3.30×10^{-2}
	1.67×10^{-7}	3.72×10^{-5}	2.47×10^{-3}	2.79×10^{-2}	3.99×10^{-5}
4	1.67×10^{1}	7.26×10^{2}	5.17×10^{4}	1.81×10^{6}	1.30×10^{7}
	4.23×10^{-7}	1.62×10^{-5}	1.00×10^{-3}	3.10×10^{-2}	9.10×10^{-1}
	2.33×10^{-8}	1.11×10^{-6}	8.65×10^{-5}	3.32×10^{-3}	2.63×10^{-2}

Table 5
Einstein *A* coefficients (first row), Franck-Condon factors (second row) and absorption band oscillator strengths (third row) for the $B^2\Sigma^+$-$A^2\Pi$ electronic transition system.

	v''				
v'	0	1	2	3	4
0	1.90×10^{3}	2.04×10^{3}	1.28×10^{3}	6.24×10^{2}	2.66×10^{2}
	1.15×10^{-1}	2.77×10^{-1}	2.97×10^{-1}	1.89×10^{-1}	7.90×10^{-2}
	2.38×10^{-6}	2.88×10^{-6}	2.05×10^{-6}	1.14×10^{-6}	5.57×10^{-7}
1	6.60×10^{3}	1.41×10^{3}	4.62×10^{0}	4.18×10^{2}	5.66×10^{2}
	2.17×10^{-1}	1.49×10^{-1}	0.00×10^{0}	1.17×10^{-1}	2.31×10^{-1}
	7.20×10^{-6}	1.72×10^{-6}	6.35×10^{-9}	6.48×10^{-7}	9.96×10^{-7}
2	1.03×10^{4}	2.83×10^{2}	2.18×10^{3}	7.10×10^{2}	3.04×10^{0}
	2.29×10^{-1}	8.00×10^{-3}	1.09×10^{-1}	9.70×10^{-2}	1.00×10^{-3}
	9.89×10^{-6}	3.03×10^{-7}	2.60×10^{-6}	9.50×10^{-7}	4.58×10^{-9}
3	9.34×10^{3}	7.09×10^{3}	1.21×10^{3}	5.73×10^{2}	1.16×10^{3}
	1.78×10^{-1}	2.70×10^{-2}	1.09×10^{-1}	3.00×10^{-3}	1.21×10^{-1}
	8.03×10^{-6}	6.74×10^{-6}	1.27×10^{-6}	6.70×10^{-7}	1.52×10^{-6}
4	5.47×10^{3}	1.56×10^{4}	1.43×10^{3}	3.30×10^{3}	3.62×10^{1}
	1.15×10^{-1}	9.50×10^{-2}	2.10×10^{-2}	8.20×10^{-2}	3.40×10^{-2}
	4.23×10^{-6}	1.32×10^{-5}	1.34×10^{-6}	3.41×10^{-6}	4.15×10^{-8}

Table 6
Radiative lifetimes (ns) of the lowest four vibrational levels for the $B^2\Sigma^+$ electronic state of SiO^+.

Vibrational level v'	This work			Exp. [21]	Exp. [28]	Cal. [27]	Cal. [25]	Cal. [23]
	Total[a]	$B^2\Sigma^+$-$X^2\Sigma^+$	$B^2\Sigma^+$-$A^2\Pi$					
0	67.8	67.8	1.59×10^5	69.5 ± 0.6	66 ± 2	77.4	59.9	72.0
1	67.6	67.6	1.01×10^5	72.4 ± 0.5		80.2	61.8	72.5
2	67.4	67.5	6.8×10^4	75.2 ± 0.5		82.9	64.0	72.7
3	67.2	67.3	4.8×10^4	78 ± 0.8				72.9

[a] Total is the lifetime of the $B^2\Sigma^+$ electronic state, the $B^2\Sigma^+$-$X^2\Sigma^+$ and $B^2\Sigma^+$-$A^2\Pi$ are the lifetimes computed assuming only the $B^2\Sigma^+$-$X^2\Sigma^+$ and $B^2\Sigma^+$-$A^2\Pi$ emission occurs.

Table 7
Radiative lifetimes for the $A^2\Pi$, $1^2\Delta$, $1^2\Sigma^-$, $2^2\Sigma^-$, $2^2\Delta$, $2^4\Sigma^+$ and $2^4\Delta$ electronic states of SiO^+.

Vibrational level v'	$A^2\Pi$/ms	$1^2\Delta$/μs	$1^2\Sigma^-$/μs	$2^2\Sigma^-$/ns	$2^2\Delta$/ns	$2^4\Sigma^+$/ns	$2^4\Delta$/ns
0	5.218	8.010	1.202	41.83	85.20	122.5	30.65
1	0.516	2.698	0.860	35.49	71.58	113.2	30.15
2	0.186			31.25	62.50	105.9	30.34
3	0.097			27.76	55.85	100.5	29.90
4	0.061			25.55	50.32	94.97	28.61

Table 8
Radiative lifetimes for the $2^2\Pi$ electronic state of SiO^+.

Vibrational level v'	$2^2\Pi$					
	Total[a]	$2^2\Pi$-$X^2\Sigma^+$/ns	$2^2\Pi$-$A^2\Pi$/μs	$2^2\Pi$-$B^2\Sigma^+$/μs	$2^2\Pi$-$1^2\Delta$/μs	$2^2\Pi$-$1^2\Sigma^-$/μs
0	51.01	52.33	2.117	50.13	832.4	625.1
1	50.44	51.65	2.291	48.86	257.3	212.4
2	50.06	51.28	2.293	48.14	113.6	89.96
3	49.60	53.03	0.797	50.16	90.68	56.56

[a] Total is the lifetime of the $2^2\Pi$ state, the $2^2\Pi$-$X^2\Sigma^+$, $2^2\Pi$-$A^2\Pi$, $2^2\Pi$-$B^2\Sigma^+$, $2^2\Pi$-$1^2\Delta$ and $2^2\Pi$-$1^2\Sigma^-$ are the lifetimes computed assuming only the $2^2\Pi$-$X^2\Sigma^+$, $2^2\Pi$-$A^2\Pi$, $2^2\Pi$-$B^2\Sigma^+$, $2^2\Pi$-$1^2\Delta$ and $2^2\Pi$-$1^2\Sigma^-$ emission occurs.

Table 9
Comparison of the Franck-Condon factors and branching ratios with previous experimental and theoretical results for the $B^2\Sigma^+(v'=0) - X^2\Sigma^+$ (v'') and $B^2\Sigma^+(v'=0) - A^2\Pi$ (v'') transitions.

	$B^2\Sigma^+(v'=0) - X^2\Sigma^+$				$B^2\Sigma^+(v'=0) - A^2\Pi$		
	$v''=0$	$v''=1$	$v''=2$	$v''=3$	$v''=0$	$v''=1$	$v''=2$
FCFs[a]	0.977	0.007	7.03E-07	8.76E-08	0.115	0.277	0.297
FCFs[b]		0.027					
FCFs[c]	0.988	0.011	0.000	0.000	0.143	0.285	0.280
FCFs[d]	0.988	0.011	0.002	0.011	0.099	0.263	0.306
$b_{v'v''}$(%)	99.7	0.23	4.58E-02	3.96E-05			
$b_{v'v''}$(%)[e]	99.6	0.1	<0.1	<0.1	<0.1	<0.1	<0.1
$b_{v'v''}$(%)[c]	97.0 + 0.7–2.5	3.0 + 0.7–0.7	<1.2	<1.2	<1.2	<0.7	<1
$b_{v'v''}$(%)[b]	97.6	2.3					

[a] FCFs: Franck-Condon factors.
[b] Calculated values from Li et al. [23].
[c] Predicted Franck-Condon factors from experimental spectra obtained by Stollenwerk et al. [28].
[d] Predicted Franck-Condon factors from experimental spectra obtained by Cameron et al. [19].
[e] Calculated branching ratio by Stollenwerk et al. [28].

MRCI/AV6Z method as implemented in MOLPRO. In this figure, the following notation is used: A–B denotes the $\langle A|H^{SO}|B\rangle$ integral. For example, the $A^2\Pi - B^2\Sigma^+$ term refers to the $\langle A^2\Pi|H^{SO}|B^2\Sigma^+\rangle$ integral. In the following, the variation of spin-orbit coupling integral versus the internuclear distance will be discussed.

As shown in Fig. 6, the values of spin-orbit coupling integral relating to the $2^2\Pi$, $2^2\Sigma^-$, $1^4\Pi$ and $2^4\Pi$ electronic states change suddenly near a certain internuclear distance. For instance, the value of $X^2\Sigma^+$-$2^2\Pi$ integral varies abruptly near R = 1.7 Å. These abrupt changes coincide with the change of the nature of the corresponding electronic wavefunctions.

Recently, Li et al. [23] had investigated the spin-orbit coupling integrals relating to the $X^2\Sigma^+$ and $B^2\Sigma^+$ electronic states for SiO^+. As shown in Fig. 2(a), the PECs of the $X^2\Sigma^+$ and $A^2\Pi$ states cross around R = 1.62 Å. The absolute value of $X^2\Sigma^+$–$A^2\Pi$ integral for R = 1.62 Å is 27 cm^{-1}, which is very close to the calculated one by Li et al. [23]. The $X^2\Sigma^+$–$A^2\Pi$ integrals for our considered internuclear distances are large enough to allow spin-orbit conversion. For the $B^2\Sigma^+$ electronic state, its PEC is crossed by those of the $1^4\Sigma^+$, $1^4\Delta$, $1^4\Sigma^-$, $1^4\Pi$, $1^2\Sigma^-$, $1^2\Delta$, $2^2\Pi$, $2^4\Sigma^-$, $2^4\Pi$ and $2^2\Sigma^-$ electronic states. But the $B^2\Sigma^+$–$1^4\Sigma^+$, $B^2\Sigma^+$–$1^4\Delta$ and $B^2\Sigma^+$–$1^2\Delta$ spin-orbit conversions are not allowed. According to the possible spin-orbit conversions, the following successive transitions are expected: $B^2\Sigma^+ \rightarrow 1^4\Sigma^- \rightarrow 1^4\Pi$.

Except for the $X^2\Sigma^+$ and $B^2\Sigma^+$ electronic states, spin-orbit coupling integrals relating to the $A^2\Pi$, $1^4\Sigma^+$, $1^4\Delta$ and $1^4\Sigma^-$ electronic

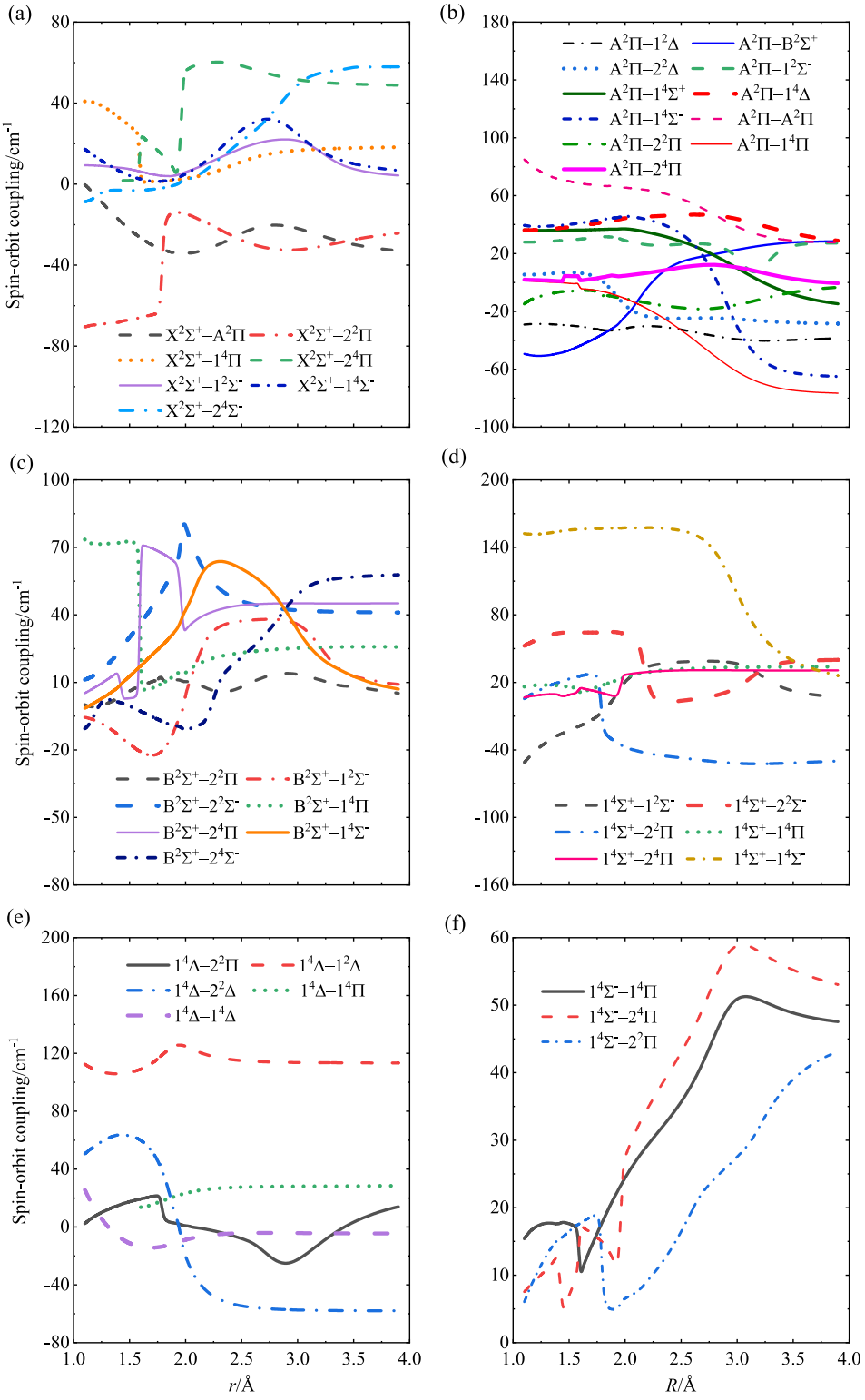

Fig. 6. Spin-orbit coupling integrals between low-lying electronic states of SiO^+.

states are also calculated in this work, just as shown in Fig. 6(b), (d), (e) and (f). For most spin-orbit couplings, their integrals are not zero at their crossings and spin-orbit conversions can occur. Such non-zero integrals along the internuclear distance mean that they are very important for accurate calculations of spectra for SiO^+.

With the consideration of the spin-orbit couplings, the 17 Λ-S states are split into 36 Ω states. Here we do not consider high-lying states. Fig. 7 shows the potential energy curves of 13 Ω states. Nine bound states are fitted to spectroscopic constants, which are presented in Table 10 and are in good agreement with available experimental and theoretical ones. By spin-orbit interactions, both

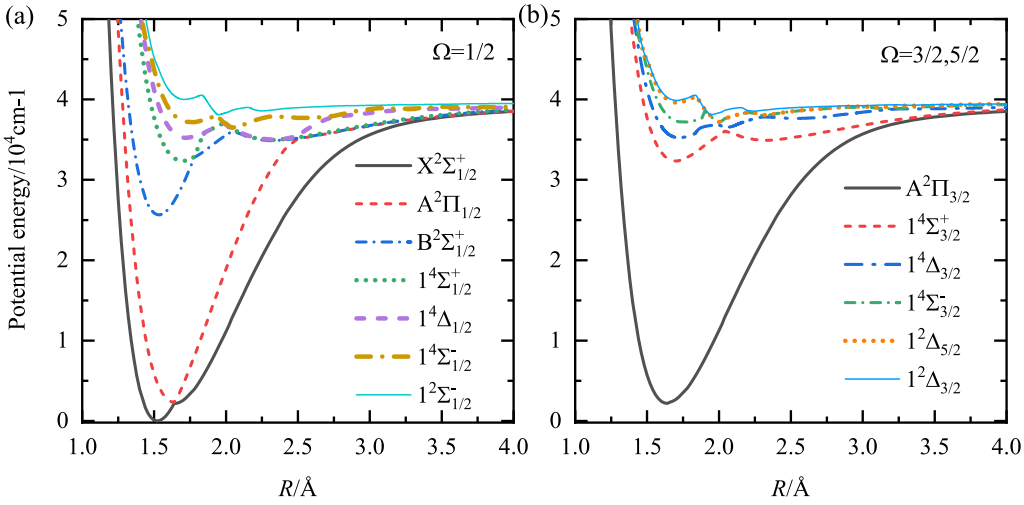

Fig. 7. Potential energy curves of low-lying Ω states of SiO^+. (a) Ω = 1/2, (b) Ω = 3/2 and 5/2.

Table 10
Comparison of spectroscopic constants for 9 bound Ω states of SiO^+ with available experimental and theoretical values.

State		T_e/cm^{-1}	R_e/Å	ω_e/cm^{-1}	$\omega_e\chi_e$/cm^{-1}	B_e/cm^{-1}
$X^2\Sigma^+_{1/2}$	This work	0.00	1.515	1165	7.34	0.7214
	Exp. [17]		1.512	1120		
	Exp. [18]			1164		0.71762
	Exp. [15]					0.7325
	Exp. [19]		1.516	1162	6.9	0.72055
	Cal. [25]		1.543	1120		
	Cal. [23]	0.00	1.523	1147	13.2	0.7155
$A^2\Pi_{1/2}$	This work	1864	1.648	935	0.04	0.6185
	Cal. [25]	810	1.655	922		
	Cal. [23]	2422	1.630	915	3.2	0.6198
$A^2\Pi_{3/2}$	This work	1746	1.629	960	13.9	0.6256
	Exp. [17]	887		1030		
	Exp. [19]	2242		944	5.0	0.6189
	Cal. [25]	781		921		
	Cal. [23]	2132		929	5.0	0.6137
$B^2\Sigma^+_{1/2}$	This work	26,024	1.522	1148	7.31	0.7141
	Exp. [17]	25,740	1.545	1180		
	Exp. [18]	26,017		1138		0.71076
	Exp. [19]	26,016		1137	6.9	0.71302
	Cal. [23]	25,575	1.533	1126	7.4	0.7048
$1^4\Sigma^+_{1/2}$	This work	33,175	1.709	921	6.65	0.5298
	Cal. [23]	32,203	1.717	984	6.0	0.5696
$1^4\Delta_{1/2}$	This work	36,233	1.726	586	10.8	0.5581
	Cal. [23]	35,318	1.730	741	0.1	0.5503
$1^4\Sigma^-_{1/2}$	This work	38,259	1.768	475	31.0	0.5306
$1^4\Sigma^+_{3/2}$	This work	33,104	1.693	739	19.1	0.5780
	Cal. [23]	32,221	1.703	743	19.9	0.5717
$1^4\Delta_{3/2}$	This work	36,236	1.725	618	24.8	0.5714
	Cal. [23]	35,315	1.730	615	23.2	0.5550

the $X^2\Sigma^+$ and $B^2\Sigma^+$ electronic states have one component noted as $X^2\Sigma^+_{1/2}$ and $B^2\Sigma^+_{1/2}$. For the ground $X^2\Sigma^+_{1/2}$ state, the differences of spectroscopic constants $\Delta\omega_e$, ΔR_e and ΔB_e produced by spin-orbit interactions are 3 cm^{-1}, 0.0008 Å and 0.0008 cm^{-1}, respectively. For the $B^2\Sigma^+_{1/2}$ state, the differences of $\Delta\omega_e$, ΔR_e, ΔB_e and ΔT_e caused by spin-orbit interactions are 1 cm^{-1}, 0.0001 Å, 0.0009 cm^{-1} and 37 cm^{-1}, respectively. The effect of spin-orbit couplings on the spectroscopic parameters for the other electronic states is also not too large. The $A^2\Pi$ electronic state is split into two components of $A^2\Pi_{1/2}$ and $A^2\Pi_{3/2}$ due to spin-orbit interactions. As shown in Fig. 7, an avoided crossing point is formed at about R = 1.65 Å between the $X^2\Sigma^+_{1/2}$ and $A^2\Pi_{1/2}$ states because they have the same Ω component of 1/2. Overall, spin-orbit couplings slightly affect the spectroscopic constants of Λ-S states around their equilibrium internuclear distances, but the shapes of the splitting states with the same Ω component may change as R is larger than that corresponds to the crossing point, just as the $X^2\Sigma^+_{1/2}$ and $A^2\Pi_{1/2}$ states.

Then we investigate the transition properties between the $X^2\Sigma^+_{1/2}$, $A^2\Pi_{1/2}$, $A^2\Pi_{3/2}$ and $B^2\Sigma^+_{1/2}$ states and determine the radiative lifetimes of the $A^2\Pi_{1/2}$, $A^2\Pi_{3/2}$ and $B^2\Sigma^+_{1/2}$ states, which are shown in Table 11. The results show that spin-orbit couplings do not have much effects on the radiative lifetimes of the $B^2\Sigma^+_{1/2}$ component.

Table 11
Radiative lifetimes (ns) of the lowest four vibrational levels for the $A^2\Pi_{1/2}$, $A^2\Pi_{3/2}$ and $B^2\Sigma^+_{1/2}$ states of SiO^+.

Vibrational level v'	Total[a]	$B^2\Sigma^+_{1/2}$- $X^2\Sigma^+_{1/2}$	$B^2\Sigma^+_{1/2}$- $A^2\Pi_{1/2}$	$B^2\Sigma^+_{1/2}$- $A^2\Pi_{3/2}$	$A^2\Pi_{1/2}$- $X^2\Sigma^+_{1/2}$	$A^2\Pi_{3/2}$- $X^2\Sigma^+_{1/2}$
0	67.6	67.7 60.1[b]	1.58×10^5 3.83×10^4[b]	1.62×10^5 3.97×10^4[b]	4.73×10^6	6.10×10^6
1	67.4	67.5 62.6[b]	1.02×10^5 4.08×10^4[b]	1.03×10^5 4.18×10^4[b]	5.33×10^5	5.21×10^5
2	67.4	67.4 64.1[b]	6.96×10^4 4.18×10^4[b]	7.04×10^4 4.37×10^4[b]	1.90×10^5	1.94×10^5
3	67.3	67.3	5.03×10^4	5.00×10^4	1.00×10^5	9.49×10^4

[a] Total is the lifetime of the $B^2\Sigma^+_{1/2}$ state, the $B^2\Sigma^+_{1/2}$- $X^2\Sigma^+_{1/2}$, $B^2\Sigma^+_{1/2}$- $A^2\Pi_{1/2}$ and $B^2\Sigma^+_{1/2}$-$A^2\Pi_{3/2}$ are the lifetimes computed assuming only the $B^2\Sigma^+_{1/2}$- $X\ ^2\Sigma^+_{1/2}$, $B^2\Sigma^+_{1/2}$- $A^2\Pi_{1/2}$ and $B^2\Sigma^+_{1/2}$-$A^2\Pi_{3/2}$ emission occurs.
[b] Values from Ref. [25].

Our results are in good agreement with those calculated by Chattopadhyaya et al [25].

4. Conclusions

In this work, the PECs of seventeen low-lying electronic states, including the newly identified $2^4\Sigma^+$, $2^4\Pi$ and $2^4\Delta$, are calculated by the icMRCI + Q/56 + CV + DK method. The fitted spectroscopic parameters are in good agreement with available experimental and theoretical ones. The TDMs for dipole allowed transitions are evaluated by the icMRCI/AV6Z approach. The PECs and TDMs are utilized to compute the Einstein *A* coefficients, Franck-Condon factors and absorption band oscillator strengths for dipole-allowed transitions, thus obtaining the radiative lifetimes of some excited states. Our calculations show that the radiative lifetime of 67.8 ns for $B^2\Sigma^+$ ($v' = 0$) is in better agreement with the recent experimental measurement of 66 ± 2 ns than other theoretical results. The spin-orbit coupling integrals are evaluated using the Breit-Pauli Hamiltonian and those relating the $A^2\Pi$, $1^4\Sigma^+$, $1^4\Delta$ and $1^4\Sigma^-$ are given for the first time. The effects of spin-orbit couplings on the electronic potential energies and transition properties of SiO^+ are also presented. The results show that spin-orbit couplings do not have much effects on the radiative lifetimes of the $B^2\Sigma^+_{1/2}$ component.

CRediT authorship contribution statement

Zhi Qin: Software, Investigation, Conceptualization, Methodology, Writing - original draft. **Tianrui Bai:** Software, Investigation. **Junming Zhao:** Investigation, Writing - review & editing. **Linhua Liu:** Supervision, Funding acquisition, Methodology, Writing - review & editing.

Declaration of Competing Interest

The authors declare that they have no known competing financial interests or personal relationships that could have appeared to influence the work reported in this paper.

Acknowledgements

This work is sponsored by the National Natural Science Foundation of China under Grant no. 51336002, 51421063. We are grateful to the two anonymous reviewers who provided many helpful suggestions.

Appendix A. Supplementary material

Supplementary data to this article can be found online at https://doi.org/10.1016/j.jms.2020.111298.

References

[1] C.W. Bauschlicher Jr., The low-lying electronic states of SiO, Chem. Phys. Lett. 658 (2016) 76–79.
[2] R. Wilson, A. Penzias, K. Jefferts, M. Kutner, P. Thaddeus, Discovery of interstellar silicon monoxide, Astrophys. J. 167 (1971) L97.
[3] D.F. Dickinson, Detection of silicon monoxide at 87 GHz, Astrophys. J. 175 (1972) L43.
[4] J. Davis, G. Blair, H. Vantill, P. Thaddeus, Vibrationally Excited Silicon Monoxide In Orion Nebula, 1974..
[5] L.E. Snyder, D. Buhl, Detection of new stellar sources of vibrationally excited silicon monoxide maser emission at 6.95 millimeters, Astrophys. J. 197 (1975) 329–340.
[6] L.M. Ziurys, P. Friberg, W.M. Irvine, Interstellar SiO as a tracer of high-temperature chemistry, Astrophys. J. 343 (1989) 201–207.
[7] Q. Zhang, P.T. Ho, M. Wright, D. Wilner, SiO Emission in a Jetlike Molecular Outflow toward L1157, Astrophys. J. Lett. 451 (2) (1995) L71.
[8] S. García-Burillo, J. Martín-Pintado, A. Fuente, R. Neri, SiO chimneys and supershells in M82, Astrophys. J. Lett. 563 (1) (2001) L27.
[9] I. Jimenez-Serra, P. Caselli, J. Tan, A. Hernandez, F. Fontani, M. Butler, S. Van Loo, Parsec-scale SiO emission in an infrared dark cloud, MNRAS 406 (1) (2010) 187–196.
[10] Y.C. Minh, H.B. Liu, Y.N. Su, P.Y. Hsieh, S.Y. Liu, S.S. Kim, M. Wright, P.T.P. Ho, SiO Emission in the galactic center, Astrophys. J. 808 (1) (2015) 86.
[11] J.M.C. Plane, J.C. Gómez-Martín, W. Feng, D. Janches, Silicon chemistry in the mesosphere and lower thermosphere, J. Geophys. Res. Atmosph. 121 (7) (2016) 3718–3728.
[12] D.A. Neufeld, A. Dalgarno, Fast molecular shocks. II-Emission from fast dissociative shocks, Astrophys. J. 344 (1989) 251–264.
[13] R. Pankhurst, A complex band-spectrum associated with an oxide of silicon, Proc. Phys. Soc. 52(5) (1940) 707..
[14] L.H. Woods, On the silicon oxide bands, Phys. Rev. 63 (11–12) (1943) 426.
[15] S. Nagaraj, R. Verma, New spectrum of the SiO^+ molecule, Can. J. Phys. 46 (14) (1968) 1597–1602.
[16] T. Dunn, K. Rao, S. Nagaraj, R. Verma, New spectrum of the SiO^+ molecule—a correction, Can. J. Phys. 47 (19) (1969) 2128.
[17] E.A. Colbourn, J.M. Dyke, E.P.F. Lee, A. Morris, I.R. Trickle, The vacuum ultraviolet photoelectron spectrum of the SiO ($X^1\Sigma^+$) molecule, Mol. Phys. 35 (3) (1978) 873–882.
[18] S. Ghosh, J. Van der Linde, R. Verma, Confirmation of the SiO^+ spectrum, J. Mol. Spectrosc. 75 (2) (1979) 169–176.
[19] R. Cameron, T.J. Scholl, L. Zhang, R.A. Holt, S.D. Rosner, Fast-ion-beam laser spectroscopy of the $B^2\Sigma^+$-$X^2\Sigma^+$ and $B^2\Sigma^+$-$A^2\Pi$ systems of SiO^+: Experiment, J. Mol. Spectrosc. 169 (2) (1995) 352–363.
[20] R. Cameron, T.J. Scholl, L. Zhang, R.A. Holt, S.D. Rosner, Fast-Ion-beam laser spectroscopy of the $B^2\Sigma^+$-$X^2\Sigma^+$ and $B^2\Sigma^+$-$A^2\Pi$ systems of SiO^+: Deperturbation analysis, J. Mol. Spectrosc. 169 (2) (1995) 364–372.
[21] T.J. Scholl, R. Cameron, S.D. Rosner, R.A. Holt, Beam-laser measurements of lifetimes in SiO^+ and N_2^+, Phys. Rev. A 51 (3) (1995) 2014.
[22] S.D. Rosner, R. Cameron, T.J. Scholl, R.A. Holt, A study of the $X^2\Sigma^+$ and $A^2\Pi$ states of SiO^+ using fast-ion-beam laser spectroscopy, J. Mol. Spectrosc. 189 (1) (1998) 83–94.
[23] R. Li, X. Yuan, G. Liang, Y. Wu, J. Wang, Laser cooling of the SiO^+ molecular ion: A theoretical contribution, Chem. Phys. 110412 (2019).
[24] D.H. Shi, W.T. Li, W. Xing, J.F. Sun, Z.L. Zhu, Y.F. Liu, MRCI study on electronic spectrum of several low-lying electronic states of the SiO^+ cation, Comput. Theor. Chem. 980 (2012) 73–84.
[25] S. Chattopadhyaya, A. Chattopadhyay, K.K. Das, Electronic spectrum of SiO^+: A theoretical study, J. Mol. Struct. Theochem. 639 (1–3) (2003) 177–185.
[26] Z.-L. Cai, J.-P. François, An internally contracted multireference configuration interaction analysis of the SiO^+ $^B2^\Sigma+$-$^X2^\Sigma+$ transition moment, Chem. Phys. Lett. 282 (1) (1998) 29–38.
[27] Z.-L. Cai, J.-P. François, Ab initio study of the electronic spectrum of the SiO^+ cation, J. Mol. Spectrosc. 197 (1) (1999) 12–18.
[28] P.R. Stollenwerk, B.C. Odom, D.L. Kokkin, T. Steimle, Electronic spectroscopy of a cold SiO^+ sample: Implications for optical pumping, J. Mol. Spectrosc. 332 (2017) 26–32.

[29] E.S. Shuman, J.F. Barry, D. DeMille, Laser cooling of a diatomic molecule, Nature 467 (7317) (2010) 820.
[30] M.T. Hummon, M. Yeo, B.K. Stuhl, A.L. Collopy, Y. Xia, J. Ye, 2D magneto-optical trapping of diatomic molecules, Phys. Rev. Lett. 110 (14) (2013) 143001.
[31] J. Barry, D. McCarron, E. Norrgard, M. Steinecker, D. DeMille, Magneto-optical trapping of a diatomic molecule, Nature 512 (7514) (2014) 286.
[32] P. Yzombard, M. Hamamda, S. Gerber, M. Doser, D. Comparat, Laser cooling of molecular anions, Phys. Rev. Lett. 114 (21) (2015) 213001.
[33] L. Santos, G. Shlyapnikov, P. Zoller, M. Lewenstein, Bose-Einstein condensation in trapped dipolar gases, Phys. Rev. Lett. 85 (9) (2000) 1791.
[34] D. DeMille, Quantum computation with trapped polar molecules, Phys. Rev. Lett. 88 (6) (2002) 067901.
[35] M.A. Baranov, M. Dalmonte, G. Pupillo, P. Zoller, Condensed matter theory of dipolar quantum gases, Chem. Rev. 112 (9) (2012) 5012–5061.
[36] R.V. Krems, Cold controlled chemistry, PCCP 10 (28) (2008) 4079–4092.
[37] S. Ospelkaus, K.-K. Ni, D. Wang, M. De Miranda, B. Neyenhuis, G. Quéméner, P. Julienne, J. Bohn, D. Jin, J. Ye, Quantum-state controlled chemical reactions of ultracold potassium-rubidium molecules, Science 327 (5967) (2010) 853–857.
[38] T. Isaev, S. Hoekstra, R. Berger, Laser-cooled RaF as a promising candidate to measure molecular parity violation, Phys. Rev. A 82 (5) (2010) 052521.
[39] J.J. Hudson, D.M. Kara, I. Smallman, B.E. Sauer, M.R. Tarbutt, E.A. Hinds, Improved measurement of the shape of the electron, Nature 473 (7348) (2011) 493.
[40] D. McCarron, M. Steinecker, Y. Zhu, D. DeMille, Magnetic trapping of an ultracold gas of polar molecules, Phys. Rev. Lett. 121 (1) (2018) 013202.
[41] J. Kobayashi, K. Aikawa, K. Oasa, S. Inouye, Prospects for narrow-line cooling of KRb molecules in the rovibrational ground state, Phys. Rev. A 89 (2) (2014) 021401.
[42] V. Zhelyazkova, A. Cournol, T.E. Wall, A. Matsushima, J.J. Hudson, E. Hinds, M. Tarbutt, B. Sauer, Laser cooling and slowing of CaF molecules, Phys. Rev. A 89 (5) (2014) 053416.
[43] N. Wells, I.C. Lane, Electronic states and spin-forbidden cooling transitions of AlH and AlF, PCCP 13 (42) (2011) 19018–19025.
[44] I.C. Lane, Ultracold fluorine production via Doppler cooled BeF, PCCP 14 (43) (2012) 15078–15087.
[45] Y. You, C.-L. Yang, Q.-Q. Zhang, M.-S. Wang, X.-G. Ma, W.-W. Liu, Ab initio studies on the spin-forbidden cooling transitions of the LiRb molecule, PCCP 18 (29) (2016) 19838–19846.
[46] X. Yuan, S. Yin, Y. Shen, Y. Liu, Y. Lian, H.-F. Xu, B. Yan, Laser cooling of thallium chloride: A theoretical investigation, J. Chem. Phys. 149 (9) (2018) 094306.
[47] J.H. Nguyen, C.R. Viteri, E.G. Hohenstein, C.D. Sherrill, K.R. Brown, B. Odom, Challenges of laser-cooling molecular ions, New J. Phys. 13 (6) (2011) 063023.
[48] S.-Y. Kang, F.-G. Kuang, G. Jiang, D.-B. Li, Y. Luo, P. Feng-Hui, W. Li-Ping, W.-Q. Hu, Y.-C. Shao, Ab initio study of laser cooling of AlF+ and AlCl+ molecular ions, J. Phys. B: Atomic Mol. Opt. Phys. 50 (10) (2017) 105103.
[49] Q.-Q. Zhang, C.-L. Yang, M.-S. Wang, X.-G. Ma, W.-W. Liu, The ground and low-lying excited states and feasibility of laser cooling for GaH+ and InH+ cations, Spectrochim. Acta Part A Mol. Biomol. Spectrosc. 193 (2018) 78–86.
[50] H.J. Werner, P.J. Knowles, G. Knizia, F.R. Manby, a. others, MOLPRO 2015, a package of ab initio programs, see http://www.molpro.net. (2015)..
[51] P.J. Knowles, H.J. Werner, An efficient second-order MCSCF method for long configuration expansions, Chem. Phys. Lett. 115 (3) (1985) 259–267.
[52] H.J. Werner, P.J. Knowles, A second order multiconfiguration SCF procedure with optimum convergence, J. Chem. Phys. 82 (11) (1985) 5053–5063.
[53] P.J. Knowles, H.J. Werner, An efficient method for the evaluation of coupling coefficients in configuration interaction calculations, Chem. Phys. Lett. 145 (6) (1988) 514–522.
[54] H.J. Werner, P.J. Knowles, An efficient internally contracted multiconfiguration reference CI method, J. Chem. Phys. 89 (9) (1988) 5803–5814.
[55] D.E. Woon, T.H. Dunning, Benchmark calculations with correlated molecular wave functions. VI. Second row A_2 and first row/second row AB diatomic molecules, J. Chem. Phys. 101 (10) (1994) 8877–8893.
[56] D.E. Woon, T.H. Dunning Jr, Gaussian basis sets for use in correlated molecular calculations. V. Core-valence basis sets for boron through neon, J. Chem. Phys. 103 (11) (1995) 4572–4585.
[57] T.V. Mourik, A. Wilson, T. Dunningjr, Benchmark calculations with correlated molecular wavefunctions XIII. Potential energy curves for He_2, Ne_2 and Ar_2 using correlation consistent basis sets through augmented sextuple zeta, Mol. Phys. 96 (4) (1999) 529–547.
[58] D.G. Truhlar, Basis-set extrapolation, Chem. Phys. Lett. 294 (1–3) (1998) 45–48.
[59] K.A. Peterson, T.H. Dunning, Accurate correlation consistent basis sets for molecular core–valence correlation effects: The second row atoms Al-Ar, and the first row atoms B-Ne revisited, J. Chem. Phys. 117 (23) (2002) 10548.
[60] W.A. de Jong, R.J. Harrison, D.A. Dixon, Parallel Douglas-Kroll energy and gradients in NWChem: Estimating scalar relativistic effects using Douglas-Kroll contracted basis sets, J. Chem. Phys. 114 (1) (2001) 48–53.
[61] M. Reiher, A. Wolf, Exact decoupling of the Dirac Hamiltonian II. The generalized Douglas-Kroll-Hess transformation up to arbitrary order, J. Chem. Phys. 121 (22) (2004) 10945–10956.
[62] M. Reiher, A. Wolf, Exact decoupling of the Dirac Hamiltonian Ⅱ. The generalized Douglas-Kroll-Hess transformation up to arbitrary order, J. Chem. Phys. 121 (2004) 10945–10956.
[63] Z. Qin, J. Zhao, L. Liu, Theoretical study on low-lying electronic states of CP radical: Energy levels, Einstein coefficients, Franck-Condon factors and radiative lifetimes, J. Quantit. Spectrosc. Radiat. Transfer 230 (2019) 36–47.
[64] Z. Qin, J.M. Zhao, L.H. Liu, Energy levels, transition dipole moment, transition probabilities and radiative lifetimes for low-lying electronic states of PN, J. Quantitat. Spectrosc. Radiat. Transfer 227 (2019) 47–56.
[65] Z. Qin, J.M. Zhao, L.H. Liu, Radiative transition probabilities between low-lying electronic states of N_2, Mol. Phys. 117 (2019) 2418–2433.
[66] D.L. Kokkin, G.B. Bacskay, T.W. Schmidt, Oscillator strengths and radiative lifetimes for C_2: Swan, Ballik-Ramsay, Phillips, and $d^3\Pi g \leftarrow c^3\Sigma_u^+$ systems, J. Chem. Phys. 126 (8) (2007) 084302.
[67] D.H. Shi, W.T. Li, J.F. Sun, Z.L. Zhu, Theoretical study of spectroscopic and molecular properties of several low-lying electronic states of CO molecule, Int. J. Quantum Chem. 113 (7) (2013) 934–942.
[68] S.D.R. Vamhindi, M. Nsangou, Accurate ab initio potential energy curves and spectroscopic properties of the low-lying electronic states of OH^- and SH^- molecular anions, Mol. Phys. 114 (14) (2016) 2204–2216.
[69] A. Berning, M. Schweuzer, H.-J. Werner, P. Knowles, P. Palmieri, Spin-orbit matrix elements for internally contracted multireference configuration interaction wavefunctions, Mol. Phys. 98 (21) (2000) 1823–1833.
[70] R.J. Le Roy, LEVEL: A computer program for solving the radial Schrödinger equation for bound and quasibound levels, J. Quant. Spectrosc. Radiat. Transf. 186 (2016) 167–178.
[71] NIST, https://physics.nist.gov/PhysRefData/ASD/levels_form.html..
[72] J.H.V. Nguyen, B. Odom, Prospects for Doppler cooling of three-electronic-level molecules, Phys. Rev. A 83 (5) (2011) 053404.
[73] P.R. Stollenwerk, I.O. Antonov, B.C. Odom, IP determination and 1+1 REMPI spectrum of SiO at 210–220 nm in an ion trap: Implications for SiO+ ion trap loading, J. Mol. Spectrosc. 355 (2019) 40–45.